Mid-infrared spectra of $He–HN_2^+$ and $He_2–HN_2^+$

M. Meuwly, S. A. Nizkorodov, J. P. Maier, and E. J. Bieske[a)]
Institut für Physikalische Chemie, Universität Basel, Klingelbergstr. 80, CH-4056, Switzerland

(Received 21 August 1995; accepted 15 November 1995)

Mid-infrared vibrational spectra of $He–HN_2^+$ and $He_2–HN_2^+$ have been recorded by monitoring their photofragmentation in a tandem mass spectrometer. For $He–HN_2^+$ three rotationally resolved bands are seen: the fundamental ν_1 transition (N–H stretch) at 3158.419 ± 0.009 cm^{-1}, the $\nu_1+\nu_b$ combination band (N–H stretch plus intermolecular bend) at 3254.671 ± 0.050 cm^{-1}, and the $\nu_1+\nu_s$ combination band (N–H stretch plus intermolecular stretch) at 3321.466 ± 0.050 cm^{-1}. The spectroscopic data facilitate the development of approximate one-dimensional radial intermolecular potentials relevant to the collinear bonding of He to HN_2^+ in its (000) and (100) vibrational states. These consist of a short range potential derived from an RKR inversion of the spectroscopic data, together with a long range polarization potential generated by considering the interaction between the He atom and a set of multipoles distributed on the HN_2^+ nuclei. The following estimates for binding energies are obtained: D_0'' = 378 cm^{-1} [$He+HN_2^+(000)$], and D_0' = 431 cm^{-1} [$He+HN_2^+(100)$]. While the ν_1 band of $He_2–HN_2^+$ is not rotationally resolved, the fact that it is barely shifted from the corresponding band of $He–HN_2^+$ suggests that the trimer possesses a structure in which one of the He atoms occupies a linear proton-bound position forming a $He–HN_2^+$ core, to which a second less strongly bound He is attached. © *1996 American Institute of Physics.* [S0021-9606(96)01908-9]

I. INTRODUCTION

Dimers consisting of molecular species joined together with a He atom have commanded experimental and theoretical attention since the exploration of I_2–He via its electronic absorptions.[1] More recently, spectroscopic studies have embraced $He–Cl_2$,[2] $He–Br_2$,[3] $He–I_2$[4] through their electronic absorptions, and He–CO,[5] He–HF,[6] He–HCl,[6] $He–CO_2$,[7] and He–HCN[8] with absorptions in the infrared. Generally, He containing dimers are extremely fragile, possessing at most a few bound levels, and typically feature dissociation energies less than a few tens of wave numbers. Undoubtedly, part of the appeal in forming and characterizing these species stems from the novelty of studying intermolecular interactions involving the extremely unreactive He atom. Perhaps more importantly, their characterization furnishes information on the intermolecular potential energy surface (PES), and in so doing enhances our understanding of bimolecular energy transfer processes.

The situation regarding the spectroscopic observation of helium containing ionic complexes is somewhat less advanced than it is for their neutral counterparts. This is unfortunate given the considerable experimental[9,10] and theoretical[11] effort expended on the investigation of elastic and inelastic processes accompanying collisions between He and various molecular ions. The spectroscopic characterization of the corresponding cation dimers, which might be expected to provide useful insights into the potential energy surface governing collisional encounters, has often been hampered by experimental difficulties attending their creation and observation in a hostile plasma environment. The approach adopted in our laboratory has involved resonance enhanced photodissociation of mass selected cluster ions in a tandem mass spectrometer, with the cooled cluster ions being produced in an electron beam crossed pulsed supersonic expansion.[12] By these means, electronic absorptions of the $He_n–N_2^+$ cation complexes have been obtained to yield information on the cluster's PES.[13,14]

The current study focuses on the proton-bound $He–HN_2^+$ complex, as revealed through its mid-infrared vibrational predissociation spectrum. The subject is one of a series of small proton-bound complexes recently studied in our laboratory that includes $He–HCO^+$,[15] $Ar–HCO^+$,[16] $H_2–HCO^+$,[17] and $H_2–HN_2^+$.[18] Spectroscopic evidence shows that in all cases the complexes prefer a configuration in which the proton can be most effectively shared between the bonded moieties: linear for the rare gas containing complexes and T shaped for the H_2 containing ones. A preliminary view of $He–HN_2^+$ was provided in an earlier publication devoted to a rotational analysis of the ν_1 transition (N–H stretch).[19] It is evident from the ν_1 band that the $He–HN_2^+$ dimer is linear (or quasilinear) and possesses a relatively short, stiff intermolecular bond, with the ground state rotational and centrifugal constants implying an approximate center-of-mass intermolecular spacing of $\langle R\rangle=3.25$ Å ($\langle R\rangle\approx\langle R^{-2}\rangle^{-1/2}$), and a radial stretching force constant of at least 4.8 N/m (comparable to that of hydrogen bonded dimers, e.g., $k_{\rm int}=23.11$ N/m for HCN–HF[20]). Appreciable interaction between the inter- and intramolecular modes of the system is emphasized by the 75.5 cm^{-1} complexation induced red shift in the HN_2^+ ν_1 frequency, and a 0.04 Å contraction in the intermolecular bond accompanying ν_1 excitation.

While providing useful preliminary information concerning the $He\cdots HN_2^+$ potential, the earlier study left many questions unanswered, particular regarding the anisotropy of

[a)]Present address: School of Chemistry, The University of Melbourne, Parkville, Victoria 3052, Australia.

the intermolecular potential. For instance, it was not immediately clear to what extent the rotational and centrifugal distortion constants were influenced by the extreme angular-radial coupling of the type previously noted for the (rare gas)–HCN complexes[21] (which are isoelectronic with the (rare gas)–HN_2^+ and (rare gas)–HCO^+ ions). For these neutral systems the intermolecular bending motion is associated with large angular excursions even in the ground state. This, together with a radial equilibrium distance that is markedly shorter in the T-shaped arrangement, causes a substantial increase in the rotational constant upon excitation of the intermolecular bend ($\approx$25% for Ar–HCN[22]), and large centrifugal distortion constants, that reflect not so much a radial stretching of the intermolecular bond, but rather are a consequence of the fact that rotational motion tends to bring the HCN axis into alignment with the intermolecular axis. In order to investigate whether similar effects are of consequence in $He–HN_2^+$, we have concentrated on recording midinfrared combination bands involving the ν_1 vibration, and the intermolecular stretch and bend vibrations (ν_s and ν_b). The spectral data suggest that the bending coordinate in the ionic complex is somewhat stiffer than it is in the HCN containing neutrals and that over the range sampled by the ground and first excited intermolecular bending wave functions there is little change in the radial equilibrium distance.

Eventually it would be desirable to use spectroscopic data to construct a complete intermolecular potential energy surface for the $He\cdots HN_2^+$ interaction. Here, as a first step in this direction, we generate one dimensional (1-D) radial potentials appropriate for the interaction of He with HN_2^+ in its (000) and (100) vibrational states, proceeding in the fashion developed for constructing spectroscopically based radial potentials for neutral van der Waals complexes.[23,24] This involves partitioning the potential into short and long range portions, the former part, valid in potential regions accessed in the spectroscopic transitions, being determined empirically by direct inversion of spectroscopic data using the rotational RKR procedure,[23] while the long range part is assumed to have a form consistent with the long range polarization interaction. The 1-D potentials enable one to estimate properties of the complex that have not yet been measured, including its dissociation energy and frequencies for higher intermolecular stretching states.

One advantage of undertaking spectroscopic explorations of ionic clusters in a mass spectrometer system is the ease and security with which the consequences of stepwise solvation can be explored. Recently we have investigated such effects in the $Ar_n–HCO^+$ ($n=1–13$) series, focusing on the development with solvent atom number of the ν_1 band position (solvent induced ν_1 band shift), combination band frequencies, and vibrational band shapes.[16] The data evoke a picture of the larger $Ar_n–HCO^+$ clusters as consisting of a linear proton-bound Ar–HCO^+ core surrounded by less strongly bound Ar atoms arranged in primary and secondary solvation rings. Shell closure to form an icosahedral type structure occurs at $Ar_{12}–HCO^+$. Unfortunately, attempts to carry out corresponding investigations on the $He_n–HN_2^+$ series have been frustrated by meagre ion currents for the larger clusters. Nevertheless, it has been possible to obtain a midinfrared spectrum for $He_2–HN_2^+$ which, although not rotationally resolved, is suggestive of a configuration in which one of the He atoms adopts a linear proton-bound position forming a $He–HN_2^+$ core, to which a second, more loosely bound He is attached.

II. EXPERIMENT

Spectra of $He–HN_2^+$ and $He_2–HN_2^+$ are obtained by exciting predissociative resonances in a guided ion beam apparatus. The experimental scheme has been outlined in a number of earlier papers dealing with the visible and uv dissociation of small ionic complexes,[12] with modifications to the arrangement facilitating measurements in the ir being detailed in recent publications concerning the $H_2–HCO^+$,[17] $He–HN_2^+$,[19] and $He–HCO^+$[15] complexes. Ion clusters are created in a pulsed supersonic expansion crossed by electrons issuing from twin filaments positioned close to the nozzle orifice. After extraction from the plasma via a skimmer biased at -5 V with respect to the remainder of the ion source, the ions are injected into a quadrupole mass filter where selection of the desired parent species is accomplished. The beam is then steered through 90° by a quadrupole bender and injected into an octopole ion guide where it is overlapped by the counterpropagating ir beam. Any resulting HN_2^+ photofragment ions are transmitted by a second quadrupole mass filter and are eventually sensed by a Daly scintillation detector[25] coupled to a boxcar integrator. Spectra are obtained by scanning the frequency of the light source while monitoring the HN_2^+ photofragment current. As both parent and photofragment ions are mass selected there is practically no ambiguity concerning their identities.

The light source is a commercial seeded optical parametric oscillator (OPO) system (Continuum Mirage 3000), capable of producing tuneable light in the midinfrared with a bandwidth of around 0.02 cm^{-1}. The $He–HN_2^+$ spectra are calibrated by directing some fraction of the ir light into an optoacoustic cell filled with ammonia vapour at 10 Torr (ammonia line positions are taken from Ref. 26) and by directing a fraction of the OPO oscillator output into an etalon to facilitate interpolation between ammonia peaks. As the ions pass through the octopole with 10 eV of translational energy, a small Doppler correction to the measured wave numbers is necessary ($\Delta\bar{\nu}/\nu = 4.72\times10^{-5}\sqrt{E/m}$ with E in eV, mass in u). By using the octopole ion guide as a retarding field energy analyser an energy spread of less than ±0.5 eV was determined for the parent ion beam, implying a Doppler width of less than 0.004 cm^{-1} at 3158 cm^{-1} (the ν_1 band center).

III. $He–HN_2^+$

A. Results and analysis

The $He–HN_2^+$ mid-infrared spectrum from 3100 to 3400 cm^{-1} is displayed in Fig. 1. Three rotationally resolved bands are apparent, the lowest lying one of which (3158 cm^{-1}) is easily the most intense. It has the form of a linear

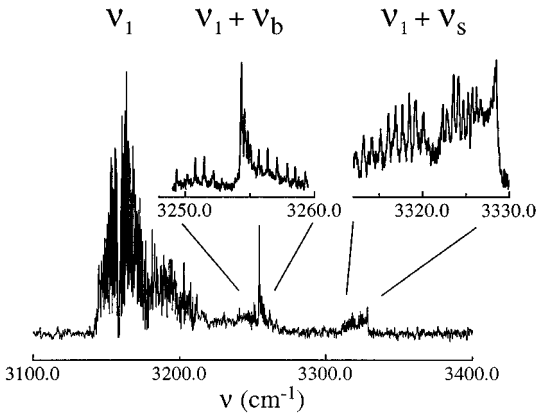

FIG. 1. Vibrational predissociation spectrum of $He–HN_2^+$ between 3100 and 3400 cm^{-1}. The spectrum was obtained by irradiating mass selected $He–HN_2^+$ complexes with photoabsorption being inferred through the detection of HN_2^+ photofragments transmitted by a second quadrupole.

molecule $\Sigma\leftarrow\Sigma$ band, features a prominent head in the *P* branch, and has been interpreted in an earlier publication as the ν_1 (N–H stretch) band.[19] The band immediately to higher energy (3255 cm^{-1}) has a noticeable *Q* branch and possesses the characteristic structure of a linear molecule perpendicular band ($\Pi\leftarrow\Sigma$ transition). The highest energy band (3321 cm^{-1}) again possesses a $\Sigma\leftarrow\Sigma$ structure though in contrast to the other $\Sigma\leftarrow\Sigma$ band, features a head in the *R* branch. Rotational line wave numbers for the $\Pi\leftarrow\Sigma$ transition and weak $\Sigma\leftarrow\Sigma$ band are provided in Tables I and II, respectively. Line positions for the ν_1 band have been given previously (Ref. 19).

The analysis of the ν_1 band (described in Ref. 19), proceeded by fitting the rotational lines to the pseudodiatomic expression

$$\nu_{\text{obs}}=\nu_0+B'[J'(J'+1)-K'^2]-D'[J'(J'+1)-K'^2]^2-B''[J''(J''+1)-K''^2]+D''[J''(J''+1)-K''^2]^2 \quad (1)$$

(with $K'=K''=0$ for the $\Sigma–\Sigma$ transition). Constants obtained from the fit are reproduced in Table III. Inclusion of higher order terms in Eq. (1) did not greatly improve fitting of line positions, with errors associated with the higher order constants exceeding the constants themselves.

For the ν_1 band, the differences between the measured line positions and those calculated using the fitted values are small, suggesting that the rotational levels of the upper state are relatively unperturbed. Interestingly, this is not the case for the corresponding transition of $He–HCO^+$ where the ν_1 rotational levels are afflicted by a series of isolated perturbations, presumably due to interaction with levels associated with intermolecular vibrations built on the (011) vibrational state of the HCO^+ core.[15]

Line positions for the $\Pi\leftarrow\Sigma$ band are listed in Table I. The *P* and *R* branch lines (which terminate in the *e* parity levels) are easily discerned, making the rotational numbering relatively straightforward. On the other hand, due to conges-

TABLE I. Wave numbers (cm^{-1}) for *P* and *R* branch rotational lines of the $He–HN_2^+$ $\nu_1+\nu_b$ band (N–H stretch in combination with the intermolecular bend). Differences between measured wave numbers and ones calculated using the fitted constants (Table III) are provided in brackets. The wave numbers of unassigned *Q* branch peaks and *Q* maximum are also provided.

J	*P*(*J*)	*R*(*J*)	Unassigned lines
0		3255.056 (29)	3254.388[a]
1		55.761 (14)	54.511
2	3252.924 (07)	56.456 (−17)	54.634
3	52.236 (06)	57.170 (−33)	54.703
4	51.529 (−22)	57.985 (48)	54.766
5	50.847 (−30)	58.611 (−60)	54.893
6	50.251 (44)	59.432 (32)	55.128
7	49.472 (−67)	60.159 (37)	55.351
8	48.893 (24)	60.812 (−21)	55.484
9	48.211 (17)	61.522 (−05)	
10			
11	46.805 (−04)		

[a]*Q* branch maximum.

TABLE II. Wave numbers (cm^{-1}) for *P* and *R* branch rotational lines of the $He–HN_2^+$ $\nu_1+\nu_s$ band (N–H stretch in combination with the intermolecular stretch). Differences between measured wave numbers and ones calculated using fitted constants (Table III) are given in brackets.

J	*P*(*J*)	*R*(*J*)
0		3322.23 (08)
1	3320.68 (−08)	22.80 (01)
2	20.08 (05)	23.46 (03)
3	19.21 (−07)	24.01 (−01)
4	18.51 (01)	24.55 (−05)
5	17.69 (−01)	25.17 (03)
6	16.90 (03)	25.64 (−02)
7	16.06 (05)	26.09 (−04)
8	15.17 (05)	26.55 (−02)
9	14.08 (−11)	26.95 (−02)
10	13.22 (−03)	27.36 (03)
11	12.33 (08)	
12	11.26 (04)	
13	10.15 (−00)	
14	09.00 (−03)	
Head		28.46

TABLE III. Fitted constants for the ground, ν_1, $\nu_1+\nu_b$, and $\nu_1+\nu_s$ levels of $He–HN_2^+$. Constants for the ground and ν_1 states are reproduced from Ref. 19. Values for the $\nu_1+\nu_b$ and $\nu_1+\nu_s$ levels were obtained by fitting *P* and *R* branch rotational line wave numbers (Table I and II) to Eq. (1), with the ground state constants fixed at the values derived from the ν_1 band analysis. The 2σ error in the final two digits of the fitted constant is given in brackets.

Vibrational level	ν_0 (cm^{-1})	*B* (cm^{-1})	*D* ($\times10^6$) cm^{-1}
0		0.3517 (05)	5.8 (0.5)
ν_1	3158.419 (09)	0.3579 (05)	3.9 (0.6)
$\nu_1+\nu_b$	3254.671 (50)	0.3559 (21)	28 (20)
$\nu_1+\nu_s$	3321.466 (50)	0.3393 (15)	18 (09)

tion in the head region, assignment of the Q branch rotational lines (accessing the f parity levels) was not possible. The ground state combination differences formed from the R and P branch lines are in good agreement with those of the ν_1 band encouraging one to presume that both bands share a common lower vibrational state. Rotational analysis proceeded by fitting the lines to expression (1) (taking $K''=0$ and $K'=1$), with the lower state constants fixed at the values determined from the ν_1 band analysis. Constants determined in this manner are provided in Table III.

Inspection of Table I shows that the deviations between the calculated and measured transition energies are in some cases quite large [e.g., ≈ -0.067 cm^{-1} for $P(7)$], with P and R branch lines terminating in a common upper state being displaced by similar amounts. This immediately suggests that several of the upper state levels are perturbed. The presence of isolated perturbations, without the observation of transitions to all interacting levels, makes it impossible to provide firm values for the $\nu_1+\nu_b$ constants (B, D, and ν_0). Future $\nu_1+\nu_b$ spectra recorded at an improved signal to noise ratio may permit the identification of transitions to the complete set of interacting levels, thereby enabling deperturbation to yield zero order constants.

It is worthwhile noting that the Q branch band shape is poorly reproduced using the constants derived from the P and R branches, with simulated contours being degraded to lower rather than to higher energy as experimentally observed. While a determination of the f manifold constants is precluded by the overlapping of lines in the head region, one obtains a much better match between the measured and calculated contours if the upper state B value is increased somewhat (to around 0.36 cm^{-1}), and the D value is decreased (to roughly 8×10^{-6} cm^{-1}).

Analysis of the weak $\Sigma\leftarrow\Sigma$ band (Fig. 1) proceeded in much the same fashion as for the $\Sigma\leftarrow\Pi$ band, although due to the band's weakness and the relatively broad rotational lines, uncertainties in line positions are larger than for the other two transitions. The line positions (Table II) were fitted to expression (1) (with $K'=K''=0$), again with the lower state parameters fixed to those determined from the main band analysis. Constants determined in the fit are listed in Table III.

We now consider in more detail the identities of the weak $\Pi\leftarrow\Sigma$ and $\Sigma\leftarrow\Sigma$ transitions. To expedite the discussion the nearby overtone and combination vibrational levels of the HN_2^+ cation are listed in Table IV. The possibility that either band is an overtone or combination band involving vibrations restricted solely to the chromophore HN_2^+ (i.e., no intermolecular motion) appears to be remote, as the appropriate higher order transitions [e.g., the $\nu_2+\nu_3\,01^{\pm1}1$ (2947 cm^{-1}), $4\nu_2\,04^00$ (2726 cm^{-1}) and perhaps $5\nu_2\,05^{\pm1}0$ ($\approx$3400 cm^{-1}) bands] are expected to be extremely weak and indeed they have not been observed for the monomer. Furthermore, in order for these levels to be responsible for the two weak bands, they would need to be shifted by several hundred wave numbers, which is improbable for a He containing complex. As well, given their large displacement from ν_1 and the tolerable agreement between the ground state combination differences for all three bands, it seems unlikely that either of the transitions is a hot band with a lower level involving intermolecular vibration (e.g., $\nu_1+\nu_s-\nu_s$ or $\nu_1+\nu_b-\nu_b$). One is thus encouraged to conclude that unless addition of a He atom leads to extraordinarily large shifts in the HN_2^+ vibrational frequencies, the two bands are due to combinations of intermolecular vibrations with ν_1. Given their energies and structures it is almost certain that they are indeed the $\nu_1+\nu_b$ (ν_1+intermolecular bend) and $\nu_1+\nu_s$ (ν_1+intermolecular stretch) combination bands.

TABLE IV. Vibrational frequencies for selected levels of the HN_2^+ cation taken from Refs. 27, 28, and 29.

Mode	Frequency (cm^{-1})
$01^{\pm1}0$	688
001	2258
04^00	2726
$04^{\pm2}0$	2749
$04^{\pm4}0$	2810
$01^{\pm1}1$	2947
100	3234
02^01	3622
$02^{\pm2}1$	3645

The occurrence of the $\nu_1+\nu_b$ band 96 cm^{-1} higher than ν_1 is surprising regarding its implication for a comparatively stiff $He\cdots HN_2^+$ bending coordinate. Normally, He containing van der Waals molecules are distinguished by the flexibility of the intermolecular bond, with the angular motion often possessing considerable free internal rotor character. If the band assignments proposed here are correct, the intermolecular bending coordinate in $He–HN_2^+$ is far more rigid than in any previously characterized He containing complex. Knowledge of the bending frequency and molecular geometry enables one to estimate the extent of the angular motion in the ground state. For an undistorted, linear HN_2^+ interacting harmonically with a He atom

$$\langle\phi^2\rangle = h/(4\pi^2\mu_b\bar{\nu}c), \tag{2}$$

where ϕ is the angle between the HN_2^+ axis and the bond between the constituents' centers of mass, $\bar{\nu}$ is the wave number of the bending vibration, and μ_b is its reduced mass. The bending reduced mass (μ_b) for the rod+ball system is given by[30]

$$\mu_b = \frac{1}{(1/I+1/(Mr^2)+1/(mr^2))}, \tag{3}$$

I being the rod's moment of inertia about its centre of mass, M the rod's mass, and m the atom's mass. Substituting the appropriate values for the $He–HN_2^+$ complex ($I=10.83$ amu Å^2, $M=29$ amu, $m=4$ amu, $r=3.2$ Å), one finds that $\mu_b=8.32$ amu Å^2 and $\langle\phi^2\rangle^{1/2}=11.8^0$. While the zero point excursion is certainly substantial, it is nonetheless significantly less than the corresponding ones for rare gas atoms bound to the isoelectronic HCN molecule (26.8^0 for Kr–HCN, 31.0^0 for Ar–HCN, 46.8^0 for Ne–HCN and essentially a free rotor for He–HCN[21]).

Excitation of the bending vibration in conjunction with ν_1 leads to the exploration of angular configurations even further from equilibrium. Assuming the small angle harmonic approximation, the average bending angle for $\nu_1+\nu_b$ can be estimated as $\langle\phi^2\rangle^{1/2}=23.6^0$. Significantly, the B values for the ν_1 manifold and the $\nu_1+\nu_b e$ parity manifold are quite close to one another, suggesting that there is little alteration in the average radial equilibrium separation as the He atom begins to traverse about the HN_2^+ core. This is in marked contrast to the situation in the Ar–HCN van der Waals molecule, where due to the combination of a sharp decrease in the radial center-of-mass minimum distance as the system moves away from linearity and an extraordinarily low bending frequency, the lowest van der Waals bending states have B values that are 25% larger than the ground state ones.[22] Unfortunately, as explained earlier, the overlapping of lines in the Q branch head region prevents a determination of the f parity manifold constants (which should not be affected by Coriolis interactions with $\nu_1+\nu_s$).

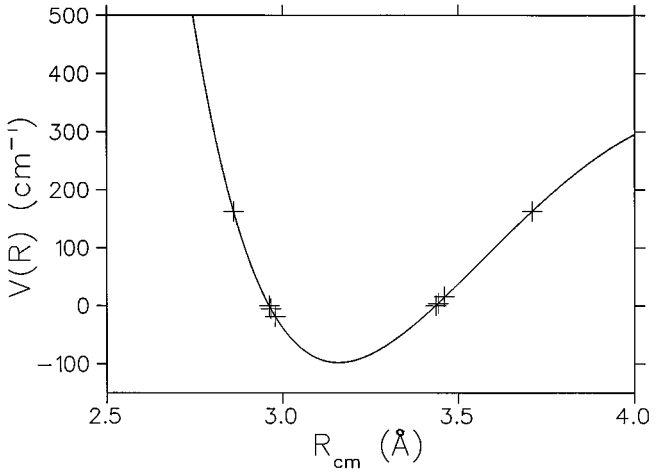

FIG. 2. Rotational RKR points for $He+HN_2^+(100)$ along with the fitted harmonic plus cubic reference potential [Eq. (5)]. The $J=0$, 10, and 20 points are shown for the $\nu_s=0$ level and the $J=0$ points for $\nu_s=1$. Parameters for the fitted reference potential are listed in Table VI.

B. One dimensional $He\cdots HN_2^+$ potentials

In this section we utilise the rotational RKR procedure [23,24] to relate the spectroscopic data for the ν_1 and $\nu_1+\nu_s$ bands to approximate radial potentials for a He atom interacting with HN_2^+ in its (000) and (100) vibrational states. Eventually, the empirical RKR potentials are extended into the asymptotic region by joining them to a theoretical long range potential appropriate for the interaction between a set of multipoles distributed over the nuclei of the HN_2^+ molecule and the polarizable He atom. This combined potential allows one to estimate properties of the complex not directly observed in the experiment, including its dissociation energy and frequencies for intermolecular stretching vibrations overtones.

Although the midinfrared spectrum contains information on intermolecular potentials relevant to the interaction of He with HN_2^+ in both its (000) and (100) states, our information for the latter is more extensive due to observation of the $\nu_1+\nu_s$ transition. This being the case, we first examine $He\cdots HN_2^+(100)$, developing potentials with and without the $\nu_1+\nu_s$ information. Having established a reasonable strategy for developing a $He\cdots HN_2^+$ potential without the $\nu_1+\nu_s$ intermolecular stretch information, we proceed to compose a potential for He interacting with HN_2^+ in its (000) state.

The rotational RKR procedure,[23,24] generates inner and outer turning points on the family of rotationally modified potentials

$$V(R;J)=V(R)+\frac{\beta^2 J(J+1)}{R_0^2+R^2}, \tag{4}$$

where R is the distance between the HN_2^+ center of mass and the He atom, $\beta=\sqrt{(h)/(8\pi^2\mu c)}$ and the quantity R_0 is related to the constituents' moments of inertia (I_1 and I_2) and reduced mass of the pseudodiatomic (μ) by $R_0=\sqrt{(I_1+I_2)/(\mu)}$. Note that the centrifugal term has been appropriately altered to take into account the extended nature of the constituents. Once they are generated it is a simple matter to relate the turning points on the rotationally corrected potentials to ones on the rotationless potential. The rotational RKR method has the advantage that the information contained in the higher order rotational constants (D, H,$\cdots$etc.) is utilised to more effectively define the inverted potential. Whereas in the traditional RKR approach a *single* pair of inner and outer turning points is produced for each vibrational state, the modified rotational RKR procedure generates a series of J dependent turning points. For a complete account of the procedure the reader should consult Refs. 23 and 24.

In order to analytically evaluate the RKR integrals it is necessary to ascertain the dependence of $E(v,J)$ and $B(v,J)$ upon the vibrational quantum number v. Initially, a harmonic approximation allows the estimation of inner and outer turning points to which an anharmonic reference potential is least square fitted. Employing this fitted reference potential, more accurate anharmonic expressions for the vibrational dependence of $E(v,J)$ and $B(v,J)$ are obtained. With these, an improved set of turning points is determined which is again fitted by a reference potential. This process is repeated until convergence is achieved. Explicit expressions for the turning points in terms of the derivatives of the reference potential and the experimentally determined rotational constants are given in Refs. 23 and 24. Here, we employ a reference potential function comprising quadratic and cubic powers of the coordinate $(r-r_e)/r$.[31] That is

$$V(r)=a+b*\left(\frac{r-r_e}{r}\right)^2+c*\left(\frac{r-r_e}{r}\right)^3. \tag{5}$$

After several iterations, the residuals of the RKR points to the fitted function were less than 0.1 cm^{-1}. The rotational RKR points and fitted potential for $He+HN_2^+(100)$ are shown in Fig. 2.

The experimental data (ν_1 and $\nu_1+\nu_s$ $J=0$–20) provide RKR turning points, and thus define the intermolecular po-

TABLE V. Atom centered spherical tensor multiple moments for the linear HN_2^+ molecule. Included are the charge (Q_0), dipole (Q_1), and quadrupole (Q_2) moments.

	N	N	H
Q_0/e	0.244	0.389	0.366
Q_1/ea_0	−0.019	0.007	0.245
Q_2/ea_0^2	−0.519	−0.193	−0.108

tential, between 2.96 and 3.71 Å. The potential can be extended to longer ranges by calculating the classical polarization energy for the $He\cdots HN_2^+$ interaction. Here, this is done by considering the induction interaction between the He atom and a set of multipoles distributed over the HN_2^+ molecule so as to mimic its charge distribution. In the present case multipoles up to quadrupole were determined using the CADPAC program package[32] and were sited on the three nuclei.

The basis functions employed in the calculation consist of a triple zeta basis set, augmented by two diffuse and one polarization function on each center: a $(10s,5p,2d,1f) \rightarrow 4s,3p,2d,1f$ plus two diffuse d and one f function with exponents 1.65, 0.469 and 1.093, respectively, on the N atoms and a $(5s,2p,1d) \rightarrow 3s,2p,1d$ plus two diffuse p and one d function with exponents 1.407, 0.388, and 1.057, respectively, on the H atom. There was no great difference between multipoles calculated with HN_2^+ bondlengths frozen at the experimental equilibrium distances (r_{NN}=1.097 Å, r_{NH}=1.033 Å), and with the optimized *ab initio* geometry (r_{NN}=1.102 Å, r_{NH}=1.031 Å). The distributed spherical tensor multipoles (up to quadrupole) are provided in Table V.

The electrical potential arising from a set of atom-centred, spherical tensor multipoles located at different locations **S**, can be written as[33]

$$\phi(\mathbf{r}) = \sum_{LM} |\mathbf{r}-\mathbf{S}|^{-L-1} Q_{LM}(\mathbf{S}) [4\pi/(2L+1)]^{1/2} Y_{LM}(\mathbf{r}-\mathbf{S})^*, \tag{6}$$

where $Y_{LM}(\mathbf{r}-\mathbf{S})$ are spherical harmonics. The polarization contribution to the long range intermolecular $He\cdots HN_2^+$ potential energy is related to the electric field by

$$V_{\text{ind}}(r,\theta) = -\tfrac{1}{2}\,\alpha \mathbf{E}(r,\theta)^2 \tag{7}$$

where α is the dipole polarizability of He [0.2048 $Å^3$ (Ref. 34)]. Eventually the $He\cdots HN_2^+$ polarization potential at θ=0 was fitted to a power series in $1/r$ (r being the distance between the He atom and the HN_2^+ center of mass),

$$V_{\text{ind}}(r) = c_0 + \sum_{n=2}^{4} \frac{c_{2n}}{r^{2n}} \tag{8}$$

with termination of the expansion at n=4 providing more than sufficient accuracy. The c_0 value is adjusted so that the polarization potential meets the RKR potential at the outermost turning point.

TABLE VI. Parameters for the $He+HN_2^+(100)$ and $He+HN_2^+(000)$ 1-D radial potentials described in the text. The complete potentials consist of a short range part [Eq. (5)], determined from the spectroscopic data via the rotational RKR procedure, joined to a long range polarization part, with the two portions connected together at the outermost RKR turning point. For $He+HN_2^+(100)$ two RKR potentials were generated, one using the ν_1 and $\nu_1+\nu_s$ data (column 2), the other with only the ν_1 data (column 3). For $He+HN_2^+(000)$ the potential was constructed using only the data pertaining to the ν_s=0 level (column 4).

	$He+HN_2^+(100)$ ν_1 and $\nu_1+\nu_s$	$He+HN_2^+(100)$ ν_1	$He+HN_2^+(000)$
r_1 (Å)	3.71	3.46	3.53
w	10	10	10
a (cm^{-1})	−97.97	−97.32	−78.38
b (cm^{-1})	18 987.2	20 490.68	13 609.21
c (cm^{-1})	−47 968.0	−27 836.57	−18 144.98
r_e (Å)	3.159	3.180	3.210
c_0 (cm^{-1})	421.16	424.04	373.14
c_4 (cm^{-1} Å^4)	-3.6×10^4	-3.6×10^4	-3.6×10^4
c_6 (cm^{-1} Å^6)	4.3×10^5	4.3×10^5	4.3×10^5
c_8 (cm^{-1} Å^8)	-8.2×10^6	-8.2×10^6	-8.2×10^6

The complete $He\cdots HN_2^+(100)$ potential was constructed by connecting the long range polarization potential to the converged RKR reference potential at the outermost turning point

$$V(r) = V_{\text{RKR}} \cdot f(r) + V_{\text{ind}} \cdot g(r), \tag{9}$$

where the $f(r)$ and $g(r)$ are the switching functions

$$f(r) = \tfrac{1}{2}\,(\tanh(r_j - r)*w + 1),$$

$$g(r) = \tfrac{1}{2}\,(\tanh(r - r_j)*w + 1) = f(-(r_j - r)). \tag{10}$$

Here, w is a parameter which determines the width of the switching function and r_j is the abscissa of the outermost RKR turning point. Parameters for the three potentials are provided in Table VI.

The combined RKR/polarization potential for $He+HN_2^+(100)$, constructed using the ν_1 and $\nu_1+\nu_s$ data, is shown in Fig. 3. It is interesting to note that the long range polarization potential practically coincides with the RKR curve between the ν_s=0 and ν_s=1 outer turning points, demonstrating that in this region the intermolecular potential is effectively dominated by the long range polarization interaction. This suggests that it should be possible to recover a reasonable intermolecular potential *without* the $\nu_1+\nu_s$ data. In order to test this hypothesis we proceeded to generate rotational RKR points for $He+HN_2^+(100)$ using only the ν_1 data with the optimized reference potential subsequently being joined to the long range polarization potential at the ν_s=0 outer turning point. Although there are modest differences in the predicted energy level spacings and dissociation energies for the two potentials generated with and without the $\nu_1+\nu_s$ data (see below), their general features concur remarkably well. Encouraged by this, we proceeded to construct a potential for $He+HN_2^+(000)$. Again the empirical B'' and D'' values were used to determine the rotational RKR

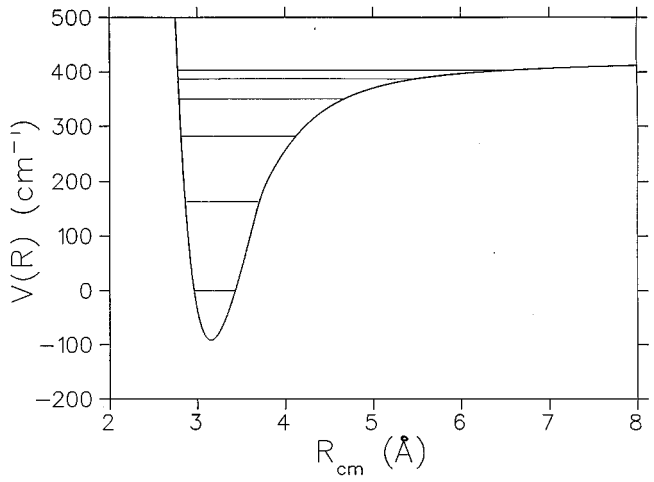

FIG. 3. One dimensional radial intermolecular potential for $He+HN_2^+(100)$ along with the six lowest vibrational levels. The potential up to the $\nu_s=1$ level was determined using the rotational RKR procedure using the ν_1 and $\nu_1+\nu_s$ data, while the long range part is due to the polarization interaction between the He atom and a set of low order multipoles sited on the HN_2^+ nuclei.

potential, which was later joined to the long range polarization potential. Complete sets of parameters for the three potentials are provided in Table VI.

In order to investigate the properties of the combined RKR/polarization potentials, the one dimensional Schrödinger equation was numerically solved in each case.[35] The predicted vibrational spacings, dissociation energies, and equilibrium distances for $He+HN_2^+(100)$ and $He+HN_2^+(000)$ are provided in Table VII. The agreement between the two $He+HN_2^+(100)$ potentials is readily apparent. While the first vibrational energy spacing for the potential derived using the ν_1 and $\nu_1+\nu_s$ data is 163.6 cm^{-1} (experimental value of 163.04 cm^{-1}) it is 174 cm^{-1} for the potential derived from the ν_1 data alone. Moreover, the D_e values for the two $He+HN_2^+(100)$ potentials are within 1 cm^{-1} of one another. The agreement is encouraging as there are proton-bound complexes for which $\nu_1+\nu_s$ stretching combination band has not yet been observed (e.g., $He–HCO+$[15]) and in the future, model potentials derived using only ν_1 data may help to focus spectroscopic searches in the appropriate region. Furthermore, the conformity of the $He+HN_2^+(100)$ potentials determined with and without the $\nu_1+\nu_s$ data can be seen as strong evidence that the weak $\Sigma–\Sigma$ band has indeed been correctly assigned as $\nu_1+\nu_s$.

The model potentials enable one to compare the interaction of HN_2^+ in its (000) and (100) states with He. This is probably most appropriately done by comparing potentials obtained without the $\nu_1+\nu_s$ data (second and third rows of Table VII). The He interaction with the vibrationally excited molecule is somewhat stronger, with a 0.03 Å shorter equilibrium intermolecular distance and 52 ± 16 cm^{-1} larger D_0 compared to the ground state molecule (the error in $D_0'-D_0''$ has been determined by calculating potentials with B and D values set to their respective error limits). While the difference in the D_0 values for the $He+HN_2^+(100)$ and $He+HN_2^+(000)$ potentials is less than the vibrational red shift ($\Delta\nu\approx75.5$ cm^{-1}), it should be remembered that the same long range polarization potential, appropriate for HN_2^+ in its equilibrium configuration, was taken for both cases, and that eventually it would be better to use vibrationally averaged moments for HN_2^+ in its (000) and (100) states. Finally it should be pointed out that the preceding development ignores coupling between the intermolecular stretching and bending motions so that the 1-D potentials developed here should be regarded as provisional. They will certainly be superseded in the future by two (and hopefully higher) dimensional surfaces.

C. Vibrational predissociation

From the rotational linewidths, it is possible to infer lower limits for the lifetime of the initially prepared state [via the relationship $\tau=(2\pi\Delta\nu)^{-1}$]. To accurately gauge the widths, slow scans at reduced power were taken over individual rotational lines (see Fig. 4). These were subsequently fitted to Lorentzian profiles to yield widths of 0.14 ± 0.02 cm^{-1} (ν_1), 0.07 ± 0.02 cm^{-1} ($\nu_1+\nu_b$) and 0.28 ± 0.08 cm^{-1} ($\nu_1+\nu_s$). No noticeable variation in the widths with rotational level was apparent in any of the three bands. If the broadening is homogeneous, the widths correspond approximately to upper state lifetimes of 38, 76, and 19 ps, respectively. While homogeneous broadening could conceivably arise either from direct coupling to the dissociative continuum (vibrational predissociation), or to a dense manifold of isoenergetic vibrational states (IVR), the latter process appears unlikely as for small systems like $He–HN_2^+$ there is unlikely to be a sufficient density of quasi-bound vibrational states isoenergetic with ν_1. A firm upper limit for the time scale of the

TABLE VII. Properties of the $He–HN_2^+$ complex determined from the collinear RKR/polarization potentials. Included are energies for the lowest five vibrational levels, dissociation energies (D_0), and radial equilibrium distances (r_e). For $He+HN_2^+(100)$ two potentials were generated, the first employing both the ν_1 and $\nu_1+\nu_s$ data, the second with only the ν_1 data. Note that the experimental $E(1,0)$ spacing for $He+HN_2^+(100)$ is 163.04 cm^{-1}.

HN_2^+ vibrational state	Levels used	D_e (cm^{-1})	D_0 (cm^{-1})	r_e (Å)	$E(1,0)$ (cm^{-1})	$E(2,0)$ (cm^{-1})	$E(3,0)$ (cm^{-1})	$E(4,0)$ (cm^{-1})	$E(5,0)$ (cm^{-1})
(100)	ν_1 and $\nu_1+\nu_s$	528.8	430.8	3.159	163.6	280.6	349.3	385.9	402.2
	ν_1	527.6	430.3	3.180	174.0	291.2	361.2	397.9	414.3
(000)	ν_1	456.8	378.4	3.210	144.9	250.8	314.5	248.2	363.2

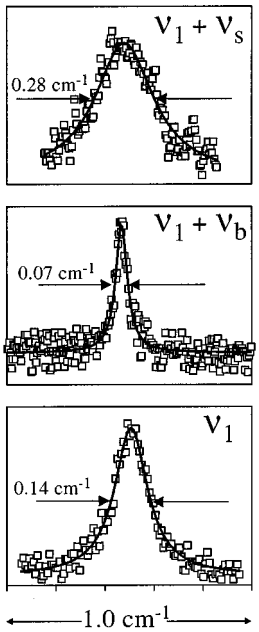

FIG. 4. Slow scans over individual rotational lines for the ν_1, $\nu_1+\nu_b$, and $\nu_1+\nu_s$ bands. The fitted Lorentzian curves have widths of 0.14 ± 0.02 cm^{-1} (ν_1), 0.07 ± 0.02 cm^{-1} ($\nu_1+\nu_b$), and 0.28 ± 0.08 cm^{-1}, respectively.

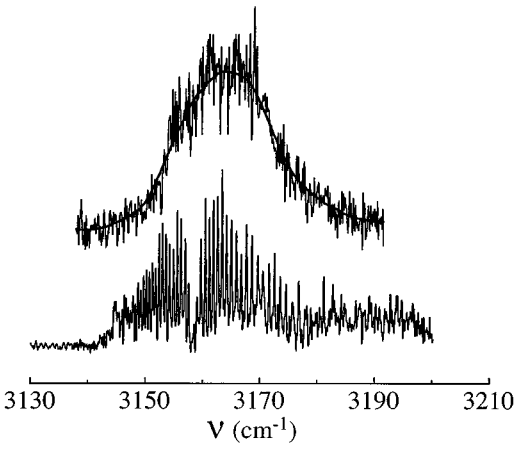

FIG. 5. Vibrational predissociation spectra of $He–HN_2^+$ and $He_2–HN_2^+$ in the ν_1 region. In both cases, the spectra were obtained by monitoring the HN_2^+ photofragment intensity.

fragmentation process is provided by the observation that the dissociation ensues on a time scale less than the ion's flight time through the octopole region of the apparatus (roughly 50 μs).

It is interesting to note the contrasting effects on the vibrational predissociation/relaxation rate caused by exciting the intermolecular stretching and bending motions in combination with ν_1. Although the precise reason for the lifetime variations is at present unclear, it is possible that the longer lifetime for the $\nu_1+\nu_b$ combination level is due to a decreased averaged projection of the N–H stretch displacement onto the intermolecular bond, while the increase in the rate for the $\nu_1+\nu_s$ combination may reflect a more favorable overlap between the bound and continuum wave functions.

IV. $He_2–HN_2^+$

Sufficient currents of the $He_2–HN_2^+$ trimer were available for its spectrum to be obtained by monitoring photofragmentation to HN_2^+ (no $He–HN_2^+$ photofragments were detected). The resulting spectrum, which is depicted along with the $He–HN_2^+$ one in Fig. 5, consists of a single broadened peak centred at 3164 ± 2 cm^{-1}, approximately 6 cm^{-1} to higher energy from the $He–HN_2^+$ ν_1 band. Significantly, the $He_2–HN_2^+$ ν_1 band lacks discernible rotational structure, despite the fact that for reasonable trimer geometries the rotational constants should be large enough for resolution of individual rotational features. It is unclear whether the absence of rotational lines is a consequence of homogeneous broadening or whether it arises from the presence of a large number of close lying sequence transitions. Conceivably both factors contribute.

While the broadened nature of the trimer spectrum makes it difficult to come to any definite conclusion concerning the arrangement of the He atoms about the HN_2^+ core, one can speculate on the basis of the relatively minor incremental band shift for the second He atom ($\approx$6 cm^{-1} to the blue) compared to the large one for the first (75.5 cm^{-1} to the red), that $He_2–HN_2^+$ possesses a structure incorporating a linear $He–HN_2^+$ core to which an extra He atom is loosely attached. That is, in both the dimer and the trimer it is a linearly disposed He atom that most influences the N–H stretching potential, with off-axis atoms having a relatively minor effect. Interestingly, the situation in the $Ar_n–HCO^+$ series, where clusters with up to 13 Ar atoms have been produced and characterized, is similar, with a huge red shift accompanying addition of the first Ar, while adding further Ar atoms results in much smaller incremental *blue* shifts.[16] This sort of behavior can be contrasted to the one found for the $Ar_n–HF$ complexes, where the incremental HF vibrational shifts resulting from the addition of the first 4 Ar atoms are all to the red: -9.6, -5.2, -4.4, and -0.4 cm^{-1}.[36]

The breakup of vibrationally excited $He_n–HN_2^+$ clusters can be compared with that of $He–N_2^+$ possessing one quantum of the N–N stretch. First one notes that vibrational relaxation is much slower for the $He_n–N_2^+$ clusters (100 μs time scale[12]) than it is for $He–HN_2^+$ prepared in the ν_1 level ($\tau_{vp}\sim$38 ps). In addition, while excitation of the ν_1 transition in $He_2–HN_2^+$ leads exclusively to HN_2^+ fragments (no $He–HN_2^+$ photofragments are observed), the $He_2–N_2^+$ ($v=1$) complexes decay into both $He–N_2^+$ and N_2^+ with a branching ratio of 55:45[37]). In the latter case the N_2^+ ($v=1$) relaxation appears to be essentially affected by a single He atom, with its prompt ejection leaving a deenergized $He–N_2^+$ fragment. Because of its much smaller mass the departing He carries away most of the vibrational energy. The rapid loss of both He atoms from $He_2–HN_2^+$ prepared in the (100) level would appear to be most consistent with a two step breakup, whereby relaxation of ν_1 is accompanied by the ejection of

the first He atom to leave the HN_2^+ core in a vibrationally excited state (perhaps with one quantum of ν_3 or several quanta of ν_2). Subsequently the second He atom is also ejected in a second relaxation/predissociation step. Such a sequential vibrational predissociation process would minimize the amount of energy flowing into the fragments' relative translational kinetic energy so avoiding energy gap bottlenecks.

V. DISCUSSION

The experimental data obtained in the present work provide a useful impression of the interaction between a He atom and HN_2^+ in the bonding region. The characteristics of the complex are usefully illuminated by comparing them with those of the neutral He–HCN van der Waals molecule (isoelectronic with $He–HN_2^+$). In contrast to the robust $He–HN_2^+$ (D_0 of approximately 380 cm^{-1}), He–HCN is extremely fragile. Although the *ab initio* He···HCN potential features an intermolecular potential well depth of 25.3 cm^{-1}, rovibrational calculations show that around 75% of this is consumed by zero point energy, and no bound intermolecular stretching states other than the ground state are predicted or indeed have been observed. The average He···HCN center-of-mass separation deduced from the experimentally obtained rotational constants (4.23 Å) is roughly 1 Å longer than it is for $He–HN_2^+$ (3.25Å).

Perhaps most surprisingly $He–HN_2^+$ features a strongly directional intermolecular bond. In contrast to He–HCN, where the intermolecular angular potential resembles an elliptical moat surrounding the rodlike HCN core,[8] the $He\cdots HN_2^+$ PES has a pronounced linear proton-bound minimum, with a relatively small zero point excursion ($\langle\phi^2\rangle^{1/2}=11.6^0$). While clearly charge-induced-dipole polarization interactions should result in significantly higher dissociation energies and intermolecular stretching frequencies for ionic rare-gas containing complexes, it is not immediately evident what influence the charge will have on the anisotropy of the intermolecular potential. In fact, from the available evidence it appears that a strongly directional intermolecular bond may be a general feature of rare-gas containing proton-bound complexes. The best documented example is $Ar–H_3^+$. There, *ab initio* calculations reveal that the Ar atom is bonded in-plane to a vertex of the H_3^+, with the barrier for planar internal rotation being roughly 1400 cm^{-1}.[38] Experimental evidence is consistent with a barrier of this magnitude, with tunneling splittings in the $Ar–H_3^+$ and $Ar–D_3^+$ microwave spectra having been effectively modeled using a barrier height of 1000 cm^{-1}.[39] It should also be remarked that not all He containing ionic complexes feature strongly directional intermolecular bonds. For example, $He–N_2^+$ has been shown through calculations[40] and spectroscopic studies[12–14] to have a PES where the intermolecular angular motion is practically unhindered and is almost a free internal rotor.

It is interesting to observe that the intermolecular bond in $He–HN_2^+$ appears to be somewhat stronger than it is in the isoelectronic $He–HCO^+$ complex,[15] as evidenced by the shorter intermolecular separation (3.25 Å compared to 3.67 Å), and smaller centrifugal distortion constant (3.9×10^{-6} cm^{-1} compared to 10.0×10^{-6} cm^{-1}). This ordering in the intermolecular bond strengths is in line with thermochemical studies which demonstrate that dissociation energies of proton-bound complexes are usually inversely correlated with the difference in the constituents' proton affinities[41] (P.A.'s: He 42.5 kcal/mol, N_2 118 kcal/mol, and CO 142 kcal/mol). As well, $He–HCO^+$ and $He–HN_2^+$ follow the trend of stronger intermolecular bonds being associated with large complexation induced redshifts in the effective proton stretching frequency (vibrational band shifts of 12.4 and 75.5 cm^{-1} respectively). This correspondence is well known in neutral hydrogen bonded systems.[42]

VI. CONCLUSIONS

The results of the current study can be summarized as follows:

(1) The B value for the ground state of $He–HN_2^+$ is consistent with a center-of-mass distance of roughly 3.25 Å with a 0.04 Å bond contraction accompanying excitation of ν_1.
(2) The presence of the He atom has a pronounced effect on the effective proton stretching potential; ν_1 in the complex is depressed by 75.5 cm^{-1} compared to free HN_2^+.
(3) The $(\nu_1+\nu_b)-\nu_1$ and $(\nu_1+\nu_s)-\nu_1$ spacings are, respectively, 96.2 and 163.0 cm^{-1}.
(4) Approximate one dimensional radial potentials for the collinear interaction of He with HN_2^+ have been developed by combining spectroscopic and theoretical data. These potentials are characterized by D_0 values of 378 and 431 cm^{-1} for HN_2^+ in its (000) and (100) states. Energies for excited intermolecular stretching states have been predicted.
(5) From individual rotational linewidths estimates for the vibrational predissociation lifetimes of 38 ps (ν_1), 76 ps ($\nu_1+\nu_b$), and 19 ps ($\nu_1+\nu_s$) are obtained.
(6) The ν_1 spectrum of $He_2–HN_2^+$ is consistent with a trimer structure whereby one of the He atoms occupies a favored linear proton-bound position to form a $He–HN_2^+$ core to which the second He is loosely attached.

ACKNOWLEDGMENTS

We are grateful for the fine technical assistance of Mr. Karl Mutschler over the course of this study. M.M. wishes to thank Prof. M. S. Child for his hospitality, since part of this work has been carried out in his group. Support through BBW Grant No. 93.02060 is acknowledged. This work is part of project No. 20-41768.94 of "Schweizerischer Nationalfonds zur Förderung der wissenschaftlichen Forschung."

[1] R. E. Smalley, D. H. Levy, and L. Wharton, J. Chem. Phys. **64**, 3266 (1976).
[2] J. I. Cline, D. D. Evard, F. Thommen, and K. C. Janda, J. Chem. Phys. **84**, 1165 (1986).
[3] L. J. van de Burgt, J. P. Nicola, and M. C. Heaven, J. Chem. Phys. **81**, 5514 (1984).
[4] D. H. Levy, Adv. Chem. Phys. **47**, 323 (1981).
[5] C. E. Chuaqui, R. J. LeRoy, and A. R. W. McKellar, J. Chem. Phys. **101**, 39 (1994).

[6] C. M. Lovejoy and D. J. Nesbitt, J. Chem. Phys. **93**, 5387 (1990).
[7] M. J. Weida, J. M. Sperhac, D. J. Nesbitt, and J. M. Hutson, J. Chem. Phys. **101**, 8351 (1994).
[8] S. Drucker, F.-M. Tao, and W. Klemperer, J. Phys. Chem. **99**, 2646 (1995).
[9] R. A. Dressler, H. Meyer, and S. R. Leone, J. Chem. Phys. **87**, 6029 (1987).
[10] M. Kriegel, R. Richter, W. Lindinger, L. Barbier, and E. E. Ferguson, J. Chem. Phys. **88**, (1988).
[11] V. A. Zenevich, W. Lindinger, and G. D. Billing, J. Chem. Phys. **97**, 7257 (1992).
[12] E. J. Bieske, Faraday Trans. **91**, 1 (1995).
[13] E. J. Bieske, A. S. Soliva, M. Welker, and J. P. Maier, J. Chem. Phys. **93**, 4477 (1990).
[14] E. J. Bieske, A. M. Soliva, A. Friedmann, and J. P. Maier, J. Chem. Phys. **96**, 28 (1992).
[15] S. A. Nizkorodov, J. P. Maier, and E. J. Bieske, J. Chem. Phys. **103**, 1297 (1995).
[16] S. A. Nizkorodov, O. Dopfer, M. Meuwly, T. Ruchti, J. P. Maier, and E. J. Bieske, J. Phys. Chem. **99**, 17118 (1995).
[17] E. J. Bieske, S. A. Nizkorodov, F. R. Bennett, and J. P. Maier, J. Chem. Phys. **102**, 5152 (1995).
[18] E. J. Bieske, S. A. Nizkorodov, F. R. Bennett, and J. P. Maier, Int. J. Mass Spectrom. Ion Processes **149/150**, 167 (1995).
[19] S. A. Nizkorodov, J. P. Maier, and E. J. Bieske, J. Chem. Phys. **102**, 5570 (1995).
[20] J. W. Bevan, in *Structure and Dynamics of Weakly Bound Molecular Complexes*, edited by A. Weber (Reidel, Dordrecht, 1987).
[21] K. R. Leopold, G. T. Fraser, S. E. Novick, and W. Klemperer, Chem. Rev. **94**, 1807 (1994).
[22] S. Drucker, A. L. Cooksy, and W. Klemperer, J. Chem. Phys. **98**, 5158 (1993).
[23] D. J. Nesbitt, M. S. Child, and D. J. Clary, J. Chem. Phys. **90**, 4855 (1989).
[24] M. S. Child and D. J. Nesbitt, Chem. Phys. Lett. **149**, 404 (1988).
[25] N. R. Daly, Rev. Sci. Instrum. **31**, 264 (1960).
[26] G. Guelachvili and K. N. Rao, *Handbook of Infrared Standards* (Academic, London, 1993).
[27] S. C. Foster and A. R. W. McKellar, J. Chem. Phys. **81**, 3424 (1984).
[28] C. S. Gudeman, M. H. Begemann, J. Pfaff, and R. J. Saykally, J. Chem. Phys. **78**, 5837 (1983).
[29] Y. Kabbadj, T. R. Huet, B. D. Rehfuss, C. M. Gabrys, and T. Oka, J. Mol. Spectrosc. **163**, 180 (1994).
[30] E. J. Bieske, M. W. Rainbird, and A. E. W. Knight, J. Chem. Phys. **94**, 7019 (1991).
[31] G. Simons, R. G. Parr, and J. M. Finlan, J. Chem. Phys. **59**, 3229 (1973).
[32] R. D. Amos, I. L. Alberts, J. S. Andrews, S. M. Colwell, N. C. Handy, D. Jayatilaka, P. J. Knowles, R. Kobayashi, N. Koga, K. E. Laidig, P. E. Maslen, C. W. Murray, J. E. Rice, J. Sanz, E. D. Simandiras, A. J. Stone, and M.-D. Su, The Cambridge Analytical Derivatives Package, Issue 5, Cambridge (1992).
[33] A. J. Stone, Chem. Phys. Lett. **83**, 233 (1981).
[34] R. R. Teachout and R. D. Pack, At. Data **3**, 195 (1971).
[35] R. J. Le Roy, University of Waterloo Chemical Physics Report CP-330 LEVEL 5.0, (1991).
[36] A. McIlroy, R. Lascola, C. M. Lovejoy, and D. J. Nesbitt, J. Phys. Chem. **95**, 2636 (1991).
[37] E. J. Bieske, S. A. Nizkorodov, A. Friedmann, and J. P. Maier, Int. J. Mass Spectr. Ion Processes **135**, 19 (1994).
[38] E. D. Simandiras, J. F. Gaw, and N. C. Handy, Chem. Phys. Lett. **141**, 166 (1987).
[39] M. Bogey, H. Bolvin, C. Demuynck, J. L. Destombes, and B. P. Van Eijck, J. Chem. Phys. **88**, 4120 (1988).
[40] S. Miller, J. Tennyson, B. Follmeg, P. Rosmus, and H. Werner, J. Chem. Phys. **89**, 2178 (1988).
[41] R. G. Keesee and A. W. Castleman, Jr., J. Phys. Chem. Ref. Data **15**, 1011 (1986).
[42] G. C. Pimental and A. L. McClellan, Annu. Rev. Phys. Chem. **22**, 347 (1971).